

# Preparing for Potential Closure of European Airspaces due to Re-entering Space Objects

Enrico Spinielli

*EUROCONTROL*

*Aviation Intelligence Unit*

Brussels, Belgium

✉ 0000-0001-8584-9131

Rainer Koelle

*EUROCONTROL*

*Aviation Intelligence Unit*

Brussels, Belgium

✉ 0000-0003-2810-1404

Quinten Goens

*EUROCONTROL*

*Aviation Intelligence Unit*

Brussels, Belgium

✉ 0000-0003-2187-1924

**Abstract**—The recent decades observed an increase in the number of space activities. This resulted in higher numbers of re-entries at the end of the respective mission lifespan or orbital decay. The risk of collision between uncontrolled re-entering space debris and aircraft is increasing due to the continual growth of flights and of orbiting bodies and their relevant re-entries. National and international authorities need to balance safety and economic impact of adopted measures. This is particularly challenging should a re-entry event be announced on short notice. Thus, there is a need for effective tools to reduce the uncertainty and increase the safety awareness of uncontrolled re-entries. To determine the risk exposure, this paper follows a data-driven approach. We employ hourly and daily spatial flight densities calculated from trajectories as recorded by EUROCONTROL’s Network Manager and binned with the Uber H3 geospatial indexing system. Impact risk probabilities are then calculated based on previous theoretical work. This work enhances the previous model by using actual flown flight trajectories as a basis for time-varying flight densities rather than relying on proxies such as the population density or ADS-B/Mode S message counts. These densities combined with a buffered area along the eventual path of re-entry, can provide mid-air impact probabilities to authorities as an aid for deciding on safety measures such as airspace closures and/or re-routings. The findings and the approach are demonstrated on the basis of an expected re-entry from an earlier space mission.

The approach in this paper enables a computing time efficient mechanism to support the re-entry related decision-making.

**Keywords**—space debris, airspace closure, aviation safety

## I. INTRODUCTION

The quest for space is a driver for technological development and exploitation. Key milestones include the first human travel to space and circumnavigating the globe, the first and now many succeeding successful landings on the moon, and regular operations of space stations in the orbit. These developments helped to identify options for the wider use of space, associated technological or operational benefits, and its commercialisation. This is showcased by an increasing number of activities aimed to generate value through the exploration of space ranging from scientific understanding and experimentation, sustainable production of goods in a non-gravity environment, space-asset based services, and recently even leisure. The increased number of launches, however, also increased the number of artefacts re-entering the atmosphere.

While ascent operations are typically well controlled and coor-

dinated, a high number of re-entries ensue based on lifespan, decay, or side-effects, such as debris, failed components, etc.

With forecasts predicting a steadily growing number of flights, see Fig. 1, and the modern race to commercialise space, there is a need to re-evaluate the risks of collision and casualties due to uncontrolled debris re-entries. The increasing risk landscape poses challenges in terms of oversight and risk management. The operational and economic demand by air transport requires a trade-off with large-scale airspace and flow management measures to address the inherent safety risk. There is a growing demand by overseeing authorities for methodologies and tools to assess which safety measures are the most adequate to minimise potential casualties and economic impact.

The increase in space operations does not exist in a vacuum. The continual growth of air traffic - despite temporal bumps - is evidenced by the surging number of flights in Europe [1] and across the world. On-going development/deployment activities of mega-constellations of satellites in Low Earth Orbit (LEO), such as the already active Starlink and OneWeb or planned ones (e.g. Kuiper, Starshield, Xingwang), will add thousand of orbiting objects, c.f. Table I with a short operational life. Some of these will inevitably re-enter the Earth’s atmosphere in an uncontrolled manner. These numbers and occurrence rates will pose challenges to the steadily increasing air traffic.

Aviation safety risk management is a well-established domain in air transportation. Despite the increasing need for situational awareness of space objects and their re-entry, the classical risk avoidance paradigm revolves around restricting the airspace. Such airspace closures impact the flow of air traffic, as the operating schedule will get distorted due to delays or re-routings circumnavigating the exposed volume of airspace. While the probability of a strike is low, it can result in catastrophic consequences. The growing number of space operations requires therefore tools to help improve the monitoring and impact of uncontrolled re-entries, techniques to help reduce the uncertainty in terms of the dimension and duration of required airspace measures, including computationally efficient and fast methods to determine the risk exposure.

This paper develops a practical and straightforward data-driven pipeline to rapidly assess the risk from uncontrolled re-entry of space debris for the European region. Apart from

the general risk assessment of potential re-entries, a soon to occur re-entry of debris from a 1972 failed USSR mission to Venus is analysed.

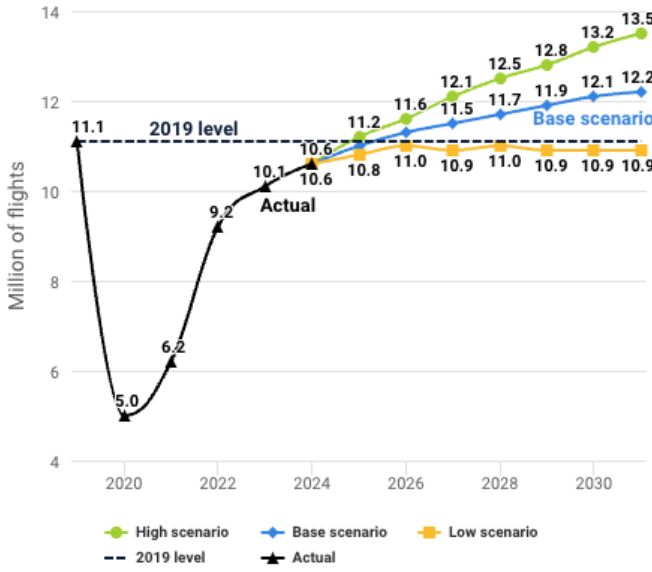


Fig. 1: EUROCONTROL 7-year forecast 2025-2031 (Spring 2025).

Constellation	Country	Launched	Active	Planned	First launch
Starlink	US	4714	3521	4714	2018
Starlink2A	US	3689	3070	6720	2022
Starlink2	US	0	0	30456	-
OneWeb	UK	660	635	716	2019
OneWeb2	UK	0	0	2304	-
Kuiper	US	29	27	3232	2023
StarShield	US	193	126	32	2022
Xingwang	CN	50	10	996	2021
Qianfan	CN	90	28	32	2024
Guangwang	CN	0	0	12992	-
Yinhe	CN	8	7	1000	2020
Hanwha	KR	0	0	2000	-
Lynk	US	10	6	2000	2020
Astra	US	0	0	13620	-
Telesat	CA	0	0	300	-
HVNET	US	0	0	1440	-
SpinLaunch	US	0	0	1190	-
Globalstar3	DE	0	0	3080	-
Honghu-3	CN	0	0	10000	-
Semaphore	FR	0	0	116640	-
E-Space	US	4	0	337323	2022

Table I: Mega-constellations (planned > 1000) as per filing to the International Telecommunication Union (ITU)

## II. METHOD

The modelling and tracking of uncontrolled re-entries poses challenges in terms of safety awareness and operational risk. Actual and historic data is sparse, and the size, shape, and attitude or rotation of re-entering objects increase the level of uncertainty for modelling. To support the decision-making, common approaches employ a mix of handling the uncertainty of object or debris movement and the associated exposed area for encounter, including temporal uncertainty windows. Thus, computationally efficient methods to assess

and continuously revalidate the collision risk of uncontrolled re-entries and aircraft will help to fine-tune the decision-making and geospatial and temporal constraints on aviation.

In general, the method for estimating the risk to commercial aircraft from re-entering debris objects revolves around estimating the exposure of a single flight and the population of flights to the re-entering object. In that respect, a robust determination of the flight density for encounter airspace volumes is a key aspect.

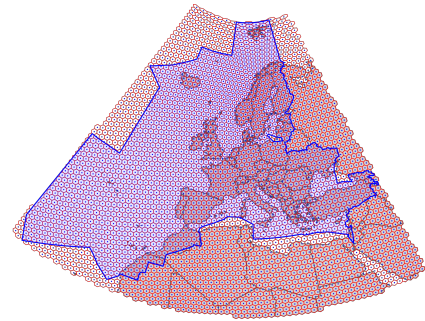


Fig. 2: H3 cells (red) at resolution 3 and their centres (blue) covering the bounding box of 43 EUROCONTROL Member States Flight Information Region (FIR)s (blue shaded polygon).

We follow the same mathematical approach of [2], [3]. However, this paper augments the approximation of risk exposure. Instead of approximating flight density with population density [2] or aircraft transponder data<sup>1</sup> [3], we use actual flown flight trajectories. This provides a more realistic figure of the number of affected air traffic. Thus, flight density is directly related to the number of flight operations per volume of airspace.

This work focusses on the European region. The hourly flight density estimation is based on *flown* Instrument Flight Rules (IFR) trajectories as recorded by EUROCONTROL's Network Manager (NM)<sup>2</sup>. These trajectories are reconstructed from the filed Flight Plan (FP) and recalculated when big deviations are detected from position reports received from Air Traffic Control (ATC).

To decrease spatial complexity, the data is binned using Uber's H3 geospatial indexing system [4]. The reduction of the spatial complexity enables fast processing. For this work, we employ a H3-cell-resolution of 3. This corresponds to hexagons of an average area 12 393 km<sup>2</sup> and an average edge length of 68.979 km [5] as depicted in Fig. 2.

The choice of hex resolution is a compromise between having to use highly detailed trajectories (more 4D positions and more processing and storage) and capturing long enough portions of flight inside the cell.

<sup>1</sup>Crowdsourced ADS-B/Mode S data suffer from lack of coverage away from landmasses and from the need to filter away position reports for stationary aircraft at airports which unnecessarily inflate the density at the location.

<sup>2</sup>NM coordinates Air Traffic Flow and Capacity Management (ATFCM) operations on behalf of EUROCONTROL's 42 Member States and 2 Comprehensive Member States covering almost all European Civil Aviation Conference (ECAC) States, see blue polygon in Fig. 2.

To build an upper threshold for the flight impact exposure, this study uses the busiest week during summer 2023 and 2024. This ensures a reasonable value, as peak airspace utilisation provides a handle on the air traffic operations and interactions of the different aircraft as part of wider ‘*traffic flows*’. The flight densities are characterised on an hourly basis for all days in these weeks per H3-cell.

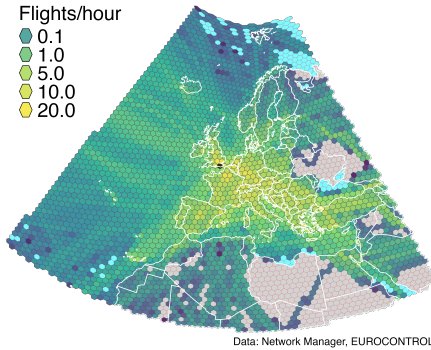


Fig. 3: Flight density in the EUROCONTROL Area on the 5th of July 2024 (the busiest day of the busiest summer week in 2024) at H3 cells resolution 3. The black hexagon in the South of UK marks the densest cell at 24.5 flights/hour, just around the airport of London Heathrow.

Fig. 3 shows an example of binning the hourly flight density on the 5th of July 2024 using H3 hexagons. The chart depicts the expected outcomes in terms of major traffic flows, and areas of high or low traffic. For example, cells with a density of zero are clearly visible for areas of war or no-fly zones (Ukraine, Libya or Syria). At the same time, the major traffic flows (North Atlantic, Canaries and East-bound over Türkiye) are clearly highlighted showing densities of more than 10.

The next sections will develop the mathematical background for the evaluation of the collision risk for which air traffic density is a key component.

#### A. Impact probability for a single flight and single debris

Safety and collision risk awareness is directly linked to the probability of a re-entering space object colliding with a traversing flight. This probability,  $p_k$ , of a debris (point) object  $k$ , impacting an aircraft (point) object over the area,  $a$ , is expressed as:

$$p_k = \varepsilon_k \int_a \rho(\vec{x}) \sigma_k(\vec{x}) da \quad (1)$$

where

- $\rho(\vec{x})$  is the probability density of an aircraft in  $\vec{x}$ ,
- $\sigma(\vec{x})$  is the impact probability density of a debris object  $k$  in the position  $\vec{x}$ , and
- $\varepsilon_k$  is the effective exposed area, i.e., the effective risk area for the  $k^{th}$  debris object impacting the aircraft (see Section II-B later on).

Our approach builds on the discretisation of the geospatial risk area. For this purpose we use a hexagon-based tessellation pattern. Uber’s H3 method ensures non-overlapping hexagons (and 12 pentagons), with an equidistant relationship between all

neighbours, and enables an efficient indexing of the cells. While this paper focusses on the determination of the risk exposure per cell, the approach would allow to identify adjacent cells to account for the inherent uncertainty and risk appetite of decision-makers.

Using H3 to discretise the area of interest  $a$  gives

$$p_k = \varepsilon_k \sum_h \rho(h) \sigma_k(h). \quad (2)$$

The impact probability  $p_k(h)$  for each cell  $h$  is determined by the following expression

$$p_k(h) = \varepsilon_k \rho(h) \sigma_k(h). \quad (3)$$

#### B. Aircraft effective exposed area

For the actual collision encounter between a re-entering object and an aircraft, we assume the aircraft impact area to be much larger than the debris object area. Thus, the area spanned by the debris object is smaller than the aircraft dimensions. This assumption holds for practically all commercial aircraft within the scope of this study, and we can neglect the debris impact area. Accordingly, we can also simplify the geometry of the aircraft and model it as a rectangular solid with dimensions of wingspan ( $W$ ), length ( $L$ ) and height ( $H$ ).

Regarding the aircraft-debris encounter geometry, this yields to two conceptual considerations:

1. if the aircraft were stationary, the area exposed to the debris impact would be the top face of the rectangular solid, and
2. if the debris were stationary, it would be the front face.

Our focus is on commercial aircraft in flight, and — implicitly — operating at higher altitudes (i.e., flight levels). The en-route portion of a flight is characterised by the aircraft in straight and level flight, moving (mainly) horizontally. At the same time, the trajectory of a falling re-entering debris object at regular en-route flight levels will be a vertical descent movement<sup>3</sup>. This encounter geometry allows to express the effective exposed area,  $\varepsilon_k$ , as

$$\varepsilon_k = \frac{s_a a_F + s_{d_k} a_T}{s_{d_k}} \quad (4)$$

where  $s_a$  is the average aircraft speed,  $s_{d_k}$  is the average fall speed of the  $k$ -th debris object,  $a_T$  area of the aircraft as viewed from the top, and  $a_F$  area of the aircraft as viewed from the front of the aircraft.

This can be further instantiated for specific aircraft types. In the calculations the following is assumed to be true ( $t$  subscript for aircraft type)

- constant debris fall speed  $s_{d_k} = 145 \text{ mph} = S$  (we adopt this value from pages 7-8 in [2])

<sup>3</sup>Even for a ballistic coefficient of  $50 \text{ lbs/ft}^2$ , the flight path angle of a re-entering object at 40 000 ft is  $-86.6^\circ$ , which corresponds to nearly vertical descent. Since most debris objects have ballistic coefficients equal to or less than  $50 \text{ lbs/ft}^2$ , the vertical descent assumption is a very accurate approximation. [2]

- constant aircraft speed,  $s_a = C_t$ , equal to its cruise speed, under the simplification that the majority of the flight time is spent cruising,
- aircraft area as viewed from the top,  $a_T = W_t \times L_t = T_t$ , where  $W_t$  is the wingspan, and  $L_t$  the length for the specific aircraft type  $t$
- aircraft area as viewed from the front,  $a_F = W_t \times H_t = F_t$ , where  $W_t$  is the wingspan, and  $H_t$  the height for the specific aircraft type  $t$

The effective exposed area now only depends on the aircraft type  $t$  (i.e., its dimensions and cruise speed) and can be rewritten as:

$$\varepsilon_t = \frac{C_t F_t + S T_t}{S} \quad (5)$$

These aircraft properties are well-known design parameters. While there does not exist a single openly available date base for these aircraft parameters, we collected the information from a series of sources and integrated them into a lookup dataset. The values  $W_t$ ,  $H_t$ ,  $L_t$  and  $C_t$  have been retrieved from [6]–[8]; we used  $\varepsilon_t = 500 \text{ m}^2$  (and  $pax = 7$ )<sup>4</sup> for missing entries which usually are due to smaller aircraft not listed in the above sources.

The impact probability for cell  $h$  under consideration of a specific aircraft of type  $t$  becomes:

$$p_{t,k}(h) = \varepsilon_t \rho_t(h) \sigma_k(h) \quad (6)$$

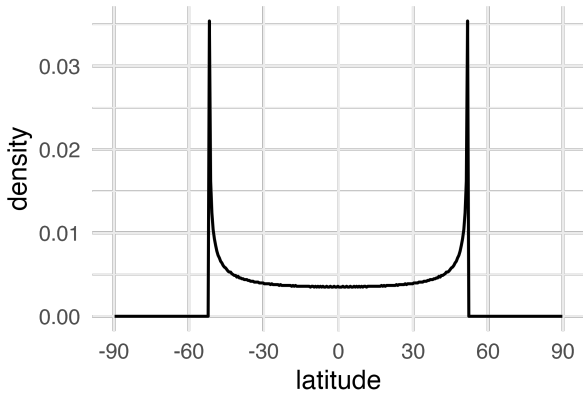


Fig. 4: Impact probability density  $\sigma(\varphi, i = 51.95)$  for debris of inclination  $i$  and altitude 550 km.

### C. Impact probability density for debris of inclination $i$

Debris that re-enter the Earth's atmosphere via drag-induced decay will fly circular orbits prior to re-entry even if initially on elliptical ones.<sup>5</sup> A characteristic point for the determination of the re-entry position is the ‘*ascending node*’. This denotes

<sup>4</sup>pax values, i.e. number of passengers, will be used for future work on casualty risk calculation.

<sup>5</sup>In fact drag at perigee will lower apogee and similarly drag at apogee will lower perigee. But because drag at perigee is higher due to denser atmosphere (the perigee is closest to Earth), the apogee will decrease faster than perigee and the orbit will then tend to become a circular one, see figure about apogee/perigee tracking in [9] for empirical evidence.

the intersection point of the object crossing the plane of Earth's equator if moving from the southern hemisphere to the northern one. The respective angular position,  $\theta = \omega + \nu$ , of the re-entry point from the ascending node, see Section VI, is uniformly distributed for uncontrolled re-entries,  $\sigma(\theta) = 1/(2\pi)$ . This is due to uncertainties in atmospheric drag and the gravitational effects of the Equatorial bulge. The height of the atmosphere is not a constant across the globe. Next to the gravitational effects, the atmosphere may also expand due to solar activity. Given these uncertainties, we assume that the impact longitude,  $\lambda$ , is uniformly distributed.

The impact probability density,  $\sigma(\varphi, i)$ , at latitude  $\varphi$  of a re-entering object whose orbit has inclination  $i$  (see Fig. 11) is given by (Equation 15 in [2]):

$$\sigma(\varphi, i) = \frac{1}{2\pi^2 R^2 \sqrt{(\sin^2(i) - \sin^2(\varphi))}} \quad (7)$$

where  $R$  is the distance from the centre of the Earth of the object potentially being impacted by the debris.

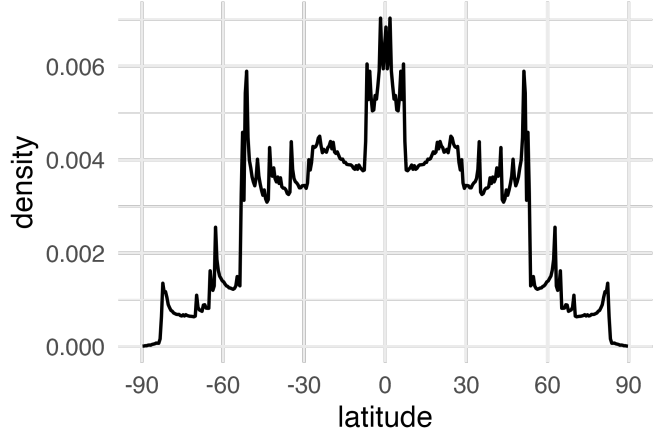


Fig. 5: Weighting function derived from 25 years of re-entries as an empirical approximation of  $\sigma(\varphi)$ .

So for example if a building is located at latitude  $30^\circ$  and has an area of  $1000 \text{ m}^2$  and a piece of debris re-enters the Earth's atmosphere from an orbit having an inclination of  $45^\circ$ , the impact probability is given by

$$P = \Delta A \times \sigma(\varphi, i) = 1000 \times \sigma\left(\frac{\pi}{6}, \frac{\pi}{4}\right) \\ = 1000 \times 2.490\,756 \times 10^{-15} = 2.490\,756 \times 10^{-12} \quad (8)$$

where we used the equatorial value of  $6378 \text{ km}$ , for the Earth's radius,  $R$ , as the distance of the building from the centre of the planet.

The impact probability density  $\sigma(\varphi, i)$  for an inclination  $i$  of  $51.95^\circ$  is plotted in Fig. 4 and takes a characteristic U shape with zero values for latitudes beyond  $i$ . This density has been derived by simulating a full circular orbit as detailed in Section VI.

#### D. Impact probability density for debris

Considering historical uncontrolled debris re-entry data, we can numerically derive the debris impact probability as a weighting function by summing up and averaging all single densities:

$$\sigma(\varphi) = \frac{1}{N} \sum_{k=1}^N \sigma(\varphi, i_k) \quad (9)$$

From [10] we extracted 1968 debris re-entries during 25 calendar years from 1st Jan 2000 till 31st Dec 2024. The result of combining all the U-shaped densities can be seen in Fig. 5.

Spatially projecting  $\sigma(\lambda, \varphi)$  on the H3 cells in the NM area, i.e. taking the mean of all the half degree weighting values and spreading in longitude, we obtain the weightings per cell (per hour  $H$ ),  $W_H(h)$ , as in Fig. 6.

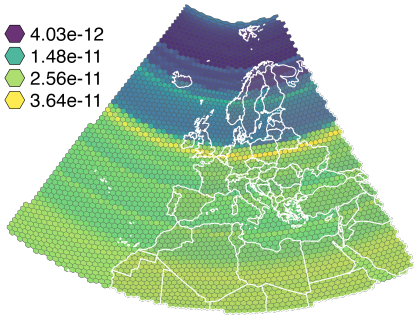


Fig. 6: Hourly weightings for H3 cells,  $W_H(h)$ , in NM area.

Then (6) becomes

$$p_t(h) = \varepsilon_t \rho_t(h) \sigma(h). \quad (10)$$

#### E. Traffic density per cell

In order to derive  $\rho_t(h)$ , we have taken the trajectories of flown flights in the NM Area, resampled at 30 s so that the calculation of the occupancy, i.e. the time spent in the hex, per aircraft type is just a matter of counting the number of points per cell. This binning operation is extremely fast to perform in Uber's H3 hierarchical geospatial indexing system and a real advantage in processing the huge amount of data point representing the flight trajectories.

For July, 5<sup>th</sup> 2024 alone, we extracted 37721 flights with 33,482,686 4D positions (at 30 s sampling), where 19 aircraft types cover each at least 1% of the total and the remaining 266 (!) types account for the residual 20.8%, see Fig. 7.

#### F. Hourly impact probability per H3 cell

When combining the hourly ( $H$ ) aircraft occupancy (per aircraft type) with the relevant weightings per  $h$  cell,  $W_H(h)$ , and the effective exposed area,  $\varepsilon_t$ , we can numerically compute the hourly impact probability for each hexagonal cell as:

$$E_{h,H} = \sum_t W_H(h) \cdot \rho_{t,H}(h) \cdot \varepsilon_t \quad (11)$$

where  $E_{h,H}$  is the collision expectation in the hexagon  $h$  at hour  $H$ .

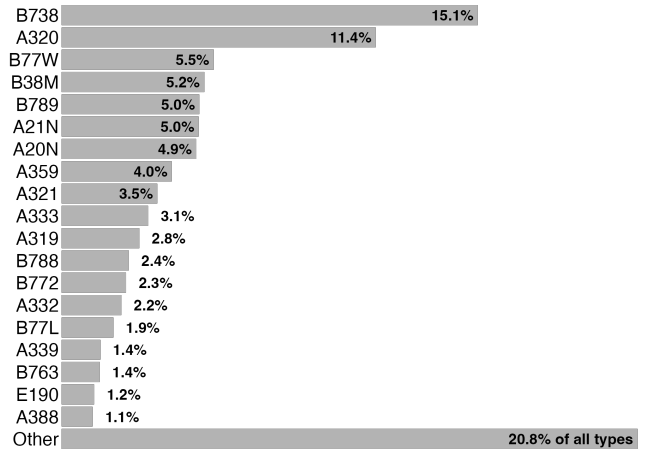


Fig. 7: Aircraft types on 2024-07-05 in NM Area.

Fig. 8 depicts the determined hourly collision expectation. As identified in Fig. 3 areas of higher traffic density observe a higher collision expectation.

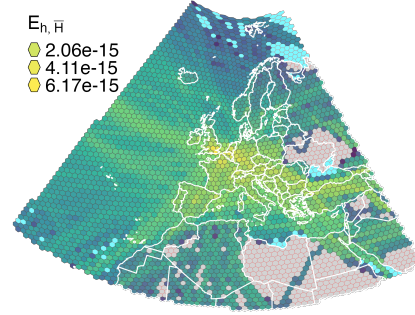


Fig. 8: Averaged hourly collision expectation on 2024-07-05.

### III. USE CASE: KOSMOS 482 DESCENT CRAFT RE-ENTRY

While this paper was being written, the KOSMOS 482 Descent Craft was being monitored for an uncontrolled re-entry, forecast at 06:39 May 10, 2025 ( $\pm 1.5$  hours) [9].

This is the lander module from a 1972 failed USSR Venera mission [11], which is reported to weigh about 480 kg and to have a diameter of approximately 1 m. Being built to survive Venus's atmosphere which is much denser and hotter than Earth's one (surface pressure 93 times that of Earth and temperatures reaching 467°C (872°F)), it could re-enter Earth intact and not break into smaller fragments some of which could burn up.

Knowing that the debris inclination is 51.95°, see Fig. 4, we can derive the maximum collision expectation using data for the busiest day in the busiest 2024 week as a proxy for the traffic density on the day of re-entry. Using the approach in this study and the weightings for this specific debris, the cell with the highest impact risk is cell, 83195dffffff (located



Fig. 9: Venera-4 lander mock-up at the Memorial Museum of Cosmonautics. The Kosmos 482 Descent Craft is probably similar.

North-West of London and overlapping with the airport of London Heathrow), with a daily value of probability collision risk of  $2.63 \cdot 10^{-10}$ . This corresponds to an annual probability of a collision between this rocket body and an aircraft of  $9.6 \cdot 10^{-8}$  (1 in 10420000). The risk is very low, for a comparison the odds of a person being struck by lightning in a given year are less than one in a million ?.

Radar systems over Germany saw the descent craft at approximately 04:30 UTC and 06:04 UTC on May 10<sup>th</sup>. Given that the descent craft was not spotted at the next expected pass at 07:32 UTC, it is likely that the re-entry already occurred before.

In general case when the re-entry track for a debris would be known with some lead time, the H3 cells around, say, 35 km on each side could be identified to retrieve the values of collision expectancy. It would then be possible to decide whether it would advisable to close the airspace and re-route traffic around the affected area.

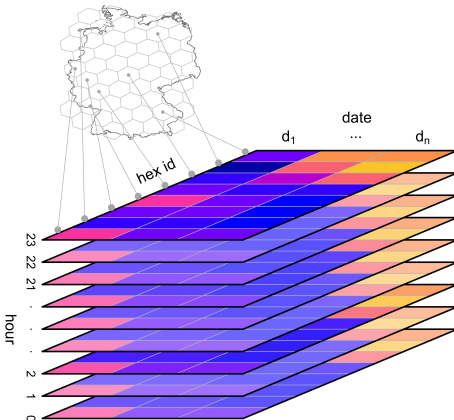


Fig. 10: Data cube of hourly flight densities data over H3 hexes (in Germany as an example) for multiple dates,  $d_1 \dots d_n$ .

#### IV. DATA AND CODE FOR REPRODUCIBILITY

We have calculated collision risk probabilities for the two busiest weeks in 2023 and 2024. The relevant dataset represents a data cube as logically depicted in Fig. 10.

The processing of data for 1 day takes less than 30 minutes from data extraction to impact probability calculation on a high-end laptop (MacBook Pro M1 Max).

Code and sample data are available in the companion GitHub repository of the paper at [https://github.com/euctrl-pru/flight\\_density\\_space\\_debris](https://github.com/euctrl-pru/flight_density_space_debris). We have also developed an R package `aviodebris` to heavy-lift the various data processing steps which is available at <https://github.com/euctrl-pru/aviodebris>.

#### V. CONCLUSION AND FUTURE WORK

Space objects and debris re-entry is an increasing risk to aviation and the general public. The higher pace of commercial space operations will see an increase of launches and subsequent re-entries. Dependent on the mission, objects re-entering the atmosphere can take on different forms, shapes, and sizes. On top, a higher number of these entries may be uncontrolled. With the continual growth of air traffic, there is a need to enhance aviation safety risk awareness and respond in a more tailored fashion to accommodate the associated uncertainties, reduce the impact on aviation, and limit the risk to the travelling public.

This paper expands on previous work. With a focus on Europe, we establish an upper bound for the traffic density based on actual flights. In particular we derive impact risk probability for the European airspace using flown trajectories.

The findings are applied to a use-case: the imminent re-entry of the lander module of an earlier failed Venus mission. The maximum collision expectation is determined using the busiest day in 2024 as a representative proxy of the traffic on the day of re-entry.

The approach presented in this paper builds on previous research. Our approach utilises H3-tessellation to reduce the spatial complexity. This cell indexing approach reduces the computation burden significantly.

Future work will address the derivation of casualty expectation using seats information for aircraft types in the traffic.

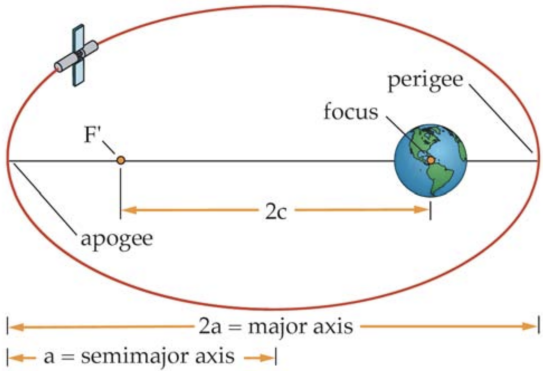
As part of this research and to inform the decision-makers it is planned to explore the impact of megaconstellations and flight growth forecast and what would happen in the mid- to long-term in various scenarios of uncontrolled re-entries and the risk for European airspace.

Of practical interest for the application of this work and future extension on casualty risk is the scenario of mission failure at launch which can typically lead to vast airspace closure and traffic re-routing: the techniques developed here would help to quantify risk and impact of the planned measures.

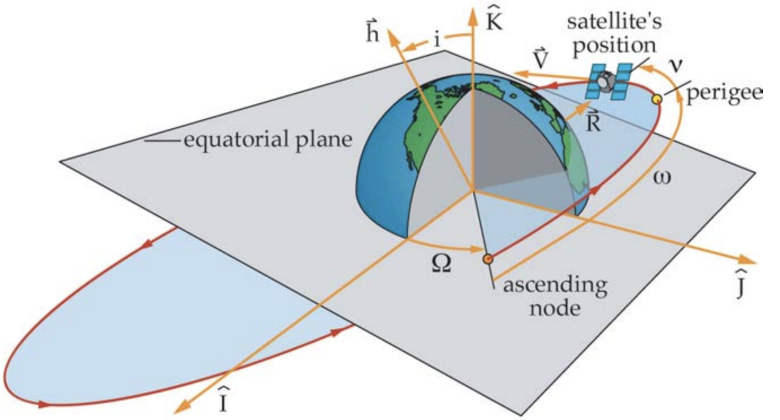
#### VI. APPENDIX: ORBITAL ELEMENTS

We refer to Fig. 11 to describe the orbital parameters of interest for the current work.

The orbital elements describing the trajectory of orbiting object are illustrated in association with an inertial reference frame  $\hat{I}\hat{J}\hat{K}$ . The  $I$ -axis,  $\hat{I}$ , points toward the vernal equinox and the  $J$ -axis,  $\hat{J}$ , is perpendicular to the  $I$ -axis in the equatorial plane in the sense of Earth's rotation, with the  $K$ -axis pointing up. The semi-major axis,  $a$ , the eccentricity,  $e$ , the inclination,  $i$ ,



(a) Keplerian elements: semi-major axis,  $a$ , the distance between the foci,  $2c$ , the eccentricity,  $e = (2c)/(2a)$ . (the semi-parameter (a.k.a. *semilatus rectum*),  $p$ , describes the size of the conic section by defining the width at the primary focus, and is defined as  $p = b^2/a = a(1 - e^2)$ )



(b) Keplerian elements: inclination,  $i$ , the right ascension of the ascending node,  $\Omega$ , and the argument of perapse,  $\omega$ . (Earth rotates around  $\hat{K}$ )

Fig. 11: Orbital elements, Figures 5-2 and 5-9 from [12].

the right ascension of the ascending node,  $\Omega$ , and the argument of perigee,  $\omega$ , constitute, together with the mean anomaly at the initial position,  $M_0$ , a set of six constants of motion that are preserved in the absence of perturbation. True anomaly,  $\nu$ , specifies the location of an orbiting object within the orbit. It is the angle between perigee and the orbiting object's position vector measured in the direction of the orbiting object's motion.

The angular position,  $\theta$ , of the re-entry debris taken from the ascending node<sup>6</sup> in the orbit plane is  $\theta = \omega + \nu$ . It is related to the latitude,  $\varphi$ , via the Cartesian coordinate  $k$ ,  $k = R \sin(\varphi) = R \sin(\theta) \sin(i)$ , or

$$\sin(\varphi) = \sin(\theta) \sin(i) \quad (12)$$

In the derivation of debris orbital positions, we use the value of the mass of Earth,  $M_{\oplus} = 5.9722 \times 10^{24}$  kg but we neglect that of the debris because many orders of magnitudes smaller (and not always known).

Of all the orbital elements, for the needs of this paper to numerically compute the weighting function, , Fig. 4, we only need the inclination  $i$ . For debris with inclination  $i$  we simulate an orbit of  $N$ , i.e. 10000, positions ( $\nu$ ) and calculate the corresponding Cartesian positions and the equivalent longitudes and latitudes. The latitudes are then binned on half degree intervals to compute  $\sigma(\varphi, i)$ , as per (7).

## REFERENCES

- [1] Statfor, “EUROCONTROL Forecast Update 2025-2031 - Spring Update | EUROCONTROL,” 28-Feb-2025. [Online]. Available: <https://www.eurocontrol.int/publication/eurocontrol-forecast-2025-2031>. [Accessed: 29-Apr-2025]
- [2] R. P. Patera, “Hazard Analysis for Uncontrolled Space Vehicle Reentry,” *Journal of Spacecraft and Rockets*, vol. 45, no. 5, pp. 1031–1041, Sep. 2008 [Online]. Available: <https://arc.aiaa.org/doi/10.2514/1.30173>. [Accessed: 23-Mar-2025]
- [3] E. Wright, A. Boley, and M. Byers, “Airspace closures due to reentering space objects,” *Sci Rep*, vol. 15, no. 1, p. 2966, Jan. 2025 [Online]. Available: <https://www.nature.com/articles/s41598-024-84001-2>. [Accessed: 06-Feb-2025]
- [4] Uber Technologies Inc., “H3: Uber’s hexagonal hierarchical spatial index.” [Online]. Available: <https://eng.uber.com/h3>
- [5] “Tables of Cell Statistics Across Resolutions | H3.” [Online]. Available: <https://h3geo.org/docs/core-library/restable>. [Accessed: 07-Feb-2025]
- [6] EUROCONTROL, “Aircraft Performance Database.” [Online]. Available: <https://contentzone.eurocontrol.int/aircraftperformance/>. [Accessed: 29-Jan-2025]
- [7] “SKYbrary Aviation Safety.” [Online]. Available: <https://skybrary.aero/>. [Accessed: 11-Apr-2025]
- [8] “Doc 8643.” [Online]. Available: <http://www.doc8643.com>. [Accessed: 11-Apr-2025]
- [9] S. Leiden, “SatTrackCam Leiden (b)log: Kosmos 482 Descent Craft reentry forecasts [UPDATED],” 24-Apr-2025. [Online]. Available: <https://sattrackcam.blogspot.com/2025/04/kosmos-842-descent-craft-reentry.html>. [Accessed: 29-Apr-2025]
- [10] J. C. McDowell, “General Catalog of Artificial Space Objects.” 2020 [Online]. Available: <https://planet4589.org/space/gcat>. [Accessed: 02-Mar-2025]
- [11] “The Space Review: Kosmos 482: Questions around a failed Venera lander from 1972 still orbiting Earth (but not for long).” [Online]. Available: <https://www.thespacereview.com/article/4384/1>. [Accessed: 30-Apr-2025]
- [12] J. J. Sellers *et al.*, *Understanding space: An introduction to astronautics*. McGraw-Hill Custom Pub., 2003 [Online]. Available: <https://books.google.be/books?id=IIcgAQAAIAAJ>

<sup>6</sup>For an earth satellite, the ascending node is the point in its orbit where a satellite crosses the equatorial plane going from south to north.